ROCK VAPOUR IS OPAQUE: IMPLICATIONS FOR DYNAMICS AND OBSERVATIONS OF LAVA PLANETS

T. GIANG NGUYEN

Department of Physics, McGill University, 3600 rue University, Montréal, QC H3A 2T8, Canada

Nicolas B. Cowan

Department of Physics, McGill University, 3600 rue University, Montréal, QC H3A 2T8, Canada and Department of Earth & Planetary Sciences, 3450 rue University, Montréal, QC H3A 0E8, Canada

Gunnar Montseny Gens

Ann and H.J. Smead Department of Aerospace Engineering Sciences, University of Colorado Boulder, 3775 Discovery Drive, Boulder, CO 80303, USA

CHARLES-ÉDOUARD BOUKARÉ

Department of Physics and Astronomy, York University, 4700 Keele St, Toronto, Ontario, Canada

WILLIAM EATON

Department of Physics, McGill University, 3600 rue University, Montréal, QC H3A 2T8, Canada

Karolina Sienko

Department of Physics, McGill University, 3600 rue University, Montréal, QC H3A 2T8, Canada Version November 18, 2025

Abstract

Extreme instellation on lava planets causes the rocky surface to melt and vaporize. Because the rock vapour composition is intrinsically tied to the mantle, atmospheric characterization of lava planets can hold valuable insight into the interior processes of rocky planets. To help interpret current data and strategize for future observations, we develop the model SonicVapour to simulate the dynamics of chemically complex secondary atmosphere of lava planets. We find that for planets with surface temperatures exceeding 2700 K, the rock vapour outgassed is optically thick, making the atmosphere vertically isothermal thus suppressing convection and severely limiting atmospheric detection via emission spectroscopy. In contrast, cooler planets with surfaces between 2300 K - 2700 K have an atmospheric opacity close to 50% and produce distinct spectral features. Counter-intuitively, therefore, cooler lava planet atmospheres are easier to detect. Our results ultimately emphasize the importance of considering atmospheric "detectability" in tandem with signal-to-noise for future observation programs.

Subject headings: Atmospheric dynamics (2300), Exoplanet atmospheres (487), Molecular spectroscopy (2095)

1. INTRODUCTION

Lava planets are rocky worlds with surface temperatures hot enough to melt their surface. Although planets such as Earth hosted global magma oceans shortly after formation, lava planets can sustain their magma oceans in perpetuity due to the sheer irradiation emitted by their host stars (Chao et al. 2021). With such intense irradiation, lava planets are prone to lose their primordial atmospheres but a secondary atmosphere can appear through the vaporization of the magma surface (Lopez et al. 2012).

The secondary rock-vapour atmosphere of a lava planet

giang.nguyen@mail.mcgill.ca

is intricately tied to its interior, so atmospheric characterization may provide information about mantle composition and dynamics (Kite et al. 2016; Boukaré et al. 2025). Lava planets therefore have been targets for many observation programs for both the Spitzer and James Webb Space Telescope: K2-141b (Zieba et al. 2022), TOI-431b (Monaghan et al. 2025), 55-cnce (Patel et al.

Atmospheric dynamics of a lava planet are unique and hard to simulate using existing frameworks. Lava planets are expected to be tidally-locked due to the close proximity to their host star, leading to a permanent dayside and nightside. This configuration can cause the secondary atmosphere to collapse on the nightside and the large pressure gradient between the two hemispheres can accelerate supersonic winds (Wordsworth 2015; Nguyen et al. 2020).

Despite the challenges of developing an accurate model for lava planet atmospheres, there have been several advancements for collapsible atmospheres with self-consistent radiative transfer for lava planets (Castan & Menou 2011; Nguyen et al. 2024). These works, however, are limited to an atmosphere consisting entirely of a single gas, e.g., Na or SiO. To fully realize the chemical complexity of lava planet atmospheres, we introduce an open-source code, SonicVapor¹, which calculates the steady-state atmospheric flow for any given magma ocean composition. We then use this model to simulate the dynamics and observations of hot and warm examples of lava planets: K2-141b and TOI-431b.

2. MODEL DESCRIPTION

2.1. Hydrodynamics

As a first order approximation, we assume that the mantles of lava planets have Bulk Silicate Earth composition with $45\%~{\rm SiO_2}, 37\%~{\rm MgO}, 8\%~{\rm FeO}$, and other trace elements (Holland & Turekian 2003). Given the magma composition, we then use the open-source code LavAtmos to find the saturated vapour pressure of the resulting outgassed atmosphere shown in Fig. 1 (Van Buchem et al. 2023).

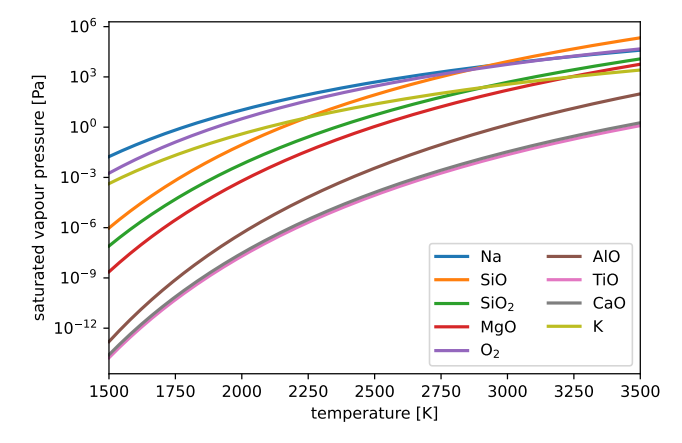


Fig. 1.— Saturated vapour pressure of nine most abundant species outgassed from Bulk Silicate Earth magma as predicted by LavAtmos (Van Buchem et al. 2023). The two most dominant species are Na which dominates at low temperatures, and SiO which dominates at high temperatures (>2800 K).

For previous modelling efforts of atmospheres with a single constituent (Nguyen et al. 2022, 2024), we isolated the saturated vapour pressure relation of either SiO or Na using chemical equilibrium models of Schaefer & Fegley (2009) or Van Buchem et al. (2023). To incorporate multiple outgassed species into the hydrodynamical framework, we must first define the total pressure, mean molecular mass, and mean specific heat capacity.

The total atmospheric pressure is simply the sum of the partial pressures: $P_{\rm tot} = \sum P_i$. The mean molecular mass is calculated via the partial pressures: $\bar{m} = (1/P_{\rm tot}) \sum P_i m_i$. The same is done for specific heat capacity: $\bar{C}_p = (1/P_{\rm tot}) \sum P_i(C_p)_i$. We can insert these

terms into the generalized system of equations as defined by the turbulent boundary layer model of Ingersoll et al. (1985) built to handle steady-state collapsible atmospheres:

$$\partial_x \left(\frac{P_{\text{tot}}}{g} V \right) = \frac{P_{\text{tot,v}} - P_{\text{tot}}}{\sqrt{2\pi R T_s}},$$
 (1)

$$\partial_x \left(\frac{P_{\text{tot}}}{g} V^2 \right) = -\partial_x \int_z P_{\text{tot}} dz + \tau,$$
 (2)

$$\partial_x \left[\frac{P_{\text{tot}}}{g} V \left(\frac{V^2}{2} + \bar{C}_p T \right) \right] = Q, \tag{3}$$

where T and T_s are atmospheric and surface temperature respectively, $P_{\rm tot,v}$ is the sum of saturated partial pressures, V is the wind speed, g is gravity, $R=k/\bar{m}$ is the gas constant, τ is drag, and Q is the energy balance of the atmosphere consisting of radiative flux and sensible heat flux. These equations are solved following Nguyen et al. (2024) and the reader can consult the appendix of that paper or the GitHub repository for how we calculate the fluxes and solve the system of equations. Solving for P, T, and V yields the pressure, temperature, and wind speed at the boundary of the turbulent layer, which is at an altitude of half the scale height (Ingersoll et al. 1985).

This new framework essentially treats an outgassed molecule as a singular species having the mean-weighted temperature-dependent properties of all the gas species. This assumes that the atmospheric mass fraction should follow the atmospheric abundances outputted by LavAtmos. Although LavAtmos outputs up to 30 gas species, we focus on the 9 species that are the most abundant and impactful for radiative transfer: Na, SiO, SiO₂, MgO, O₂, AlO, TiO, CaO, and K.

A drawback to this approach is that there is a net evaporative zone and condensation zone for the entire atmosphere whereas a realistic lava planet atmosphere should have different zones for each gas species (i.e SiO should condense at hotter temperatures than Na). Another limit is that Coriolis forcing is neglected due to the additional complexity of 3D flow instead of 2D (horizontal along co-latitudes and vertical). Nguyen et al. (2024) also included cloud formation and latent heat but these processes have only a minor impact on the atmosphere and are hard to implement for multi-component atmospheres; these processes are also neglected.

2.2. Radiative transfer

With the chemical complexity implemented into the hydrodynamical equations, we move onto the radiative transfer within the atmosphere. This is done by calculating heating by absorption of stellar and surface flux, and thermal emission of the atmosphere. The balance of these terms contribute towards solving Q in Eq. 3 and is also performed following Nguyen et al. (2024).

What is new for radiative transfer compared to previous work is that the atmosphere contains 9 gas species instead of being purely SiO. We extract absorption cross-section of each gas species from the database ExoMol (Tennyson & Yurchenko 2012), shown in Fig. 2.

Solving Equations 1-3 lets us find the total pressure and atmospheric temperature. We then calculate

https://github.com/TueGiangNguyen/SonicVapour

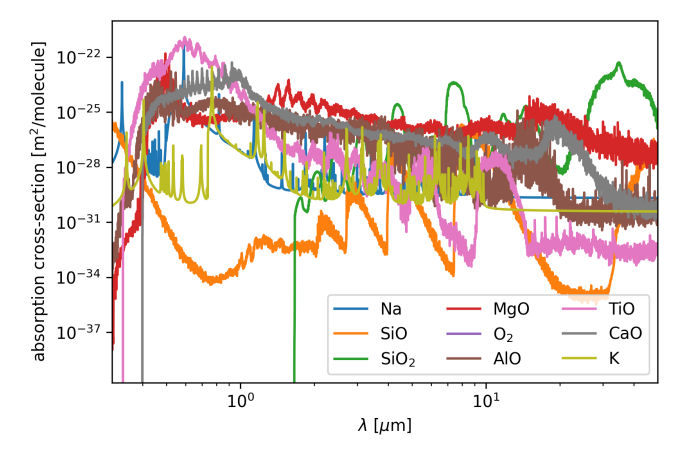


FIG. 2.— Absorption cross-section per molecule extracted from the ExoMol database. For this plot, we set the temperature to 2800 K and pressure to 7.7 kPa as thermal and pressure broadening parameters. Note that MgO has very broad peaks spanning the visible and IR and will play a large role in the atmosphere's radiative balance.

the abundance of each species using the molar mass fraction outputs of LavAtmos. These terms are then used with the absorption cross-sections to compute the opacity spectrum for the appropriate pressure and temperature broadening. We take the sum of the optical depths calculated for each species to determine the spectral opacity, $\epsilon(\lambda)$, using petitradtrans (Mollière et al. 2019).

Once the spectral opacity is found at a location, we calculate the radiative fluxes in the same manner as Nguyen et al. (2024). Stellar absorption is computed as $\int \epsilon(\lambda) F_*(\lambda) d\lambda$ where F_* is the stellar spectrum. Surface flux absorption is computed as $\pi \int \epsilon(\lambda) B(\lambda, T_s) d\lambda$ while radiative cooling is $\pi \int \epsilon(\lambda) B(\lambda, T) d\lambda$ where B is the Planck function.

Stellar data are derived from analogous stars from the MUSCLES survey (France et al. 2016): we scale the spectrum of HD85512 for K2-141 and HD40307 for TOI-431. Because of the high opacity in the visible, we also impose a vertically isothermal profile for the purposes of solving the fluid dynamics (Chandrasekhar 1947, 1960). This is also consistent with other radiative transfer simulations of lava planets (Zilinskas et al. 2022).

3. RESULTS

3.1. Model results

We used the methods described above to model the atmospheric conditions of K2-141b and TOI-431b. K2-141b is our the high-temperature case with a massive and optically thick atmosphere. TOI-431b is the low-temperature case with a much thinner atmosphere. Basic planetary parameters are shown in Table 1. The model results are shown in Figure. 3.

For K2-141b, the opacity is near unity within 40° of the sub-stellar point so the atmosphere essentially radiates like a perfect blackbody. The atmospheric temperature is the same as the surface temperature — vertically isothermal — because the atmosphere radiates to the surface as much as the surface radiates to the atmosphere. Beyond 40°, the atmosphere becomes optically thin enough that atmospheric temperature rises above surface temperatures for reasons described in Section 4.

	K2-141b	TOI-431b
Planet radius	1.54 R _⊕	1.28 R⊕
Stellar radius	0.681 R _*	0.731 R _*
Distance	2.30 a/R_*	3.32 a/R_*
Stellar temp.	4373 K	4850 K
Mass	$5.08~\mathrm{M}_E$	$3.07 M_E$
Irr. temp.	3056 K	2466 K
	Malavolta et al.	(Osborn et al.
Source	(2018)	2021)

TABLE 1

Basic properties of lava planets K2-141b and TOI-431b.

Despite orbiting a cooler star, K2-141b's proximity to its

HOST MAKES IT HOTTER.

For TOI-431b, its atmosphere is an order of magnitude less massive than K2-141b's. Because TOI-431b's atmosphere never approaches an opacity of unity, the surface is significantly cooler than the atmosphere. When comparing to previous results of TOI-431b from Nguyen et al. (2024) with an optically thin pure SiO atmosphere, the thicker atmosphere in this work cools the surface by $\sim\!\!200~\mathrm{K}$ because less visible light hits the surface.

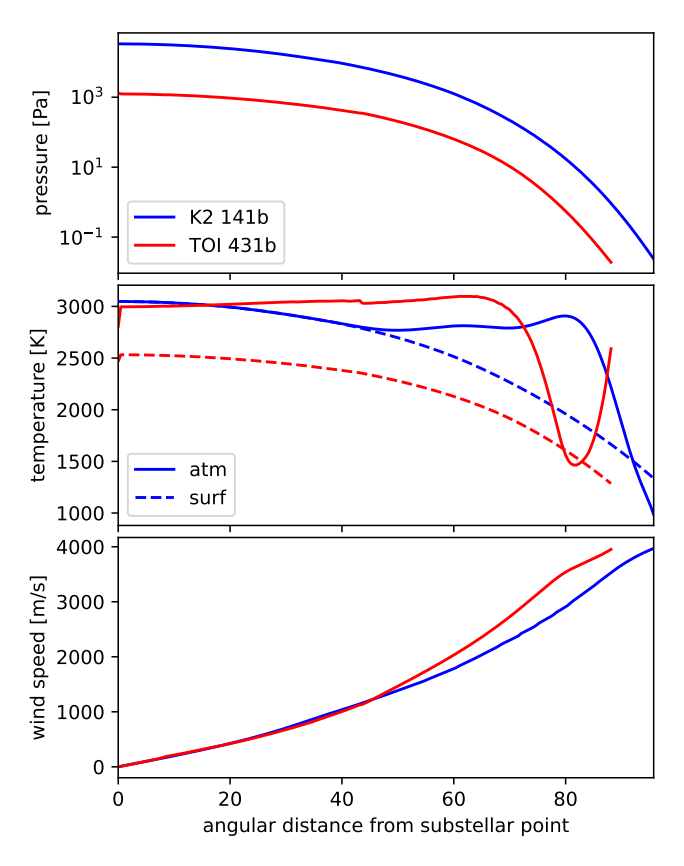


FIG. 3.— Atmospheric pressure (top), surface and atmospheric temperature (middle), and wind speeds (bottom) of K2-141b and TOI-431b at an altitude of half a scale-height. Because the surface temperature of K2-141b is hundreds of Kelvin hotter, the atmosphere of K2-141b is an order of magnitude thicker than that of TOI-431b. For K2-141b, the atmosphere shares the same temperature as the surface for much of the dayside due to the atmosphere's optical thickness. TOI-431b has an optically thinner atmosphere so there is an appreciable difference in temperature between the atmosphere and the surface. Surprisingly, both planets have similar wind speeds despite having wildly different atmospheric conditions.

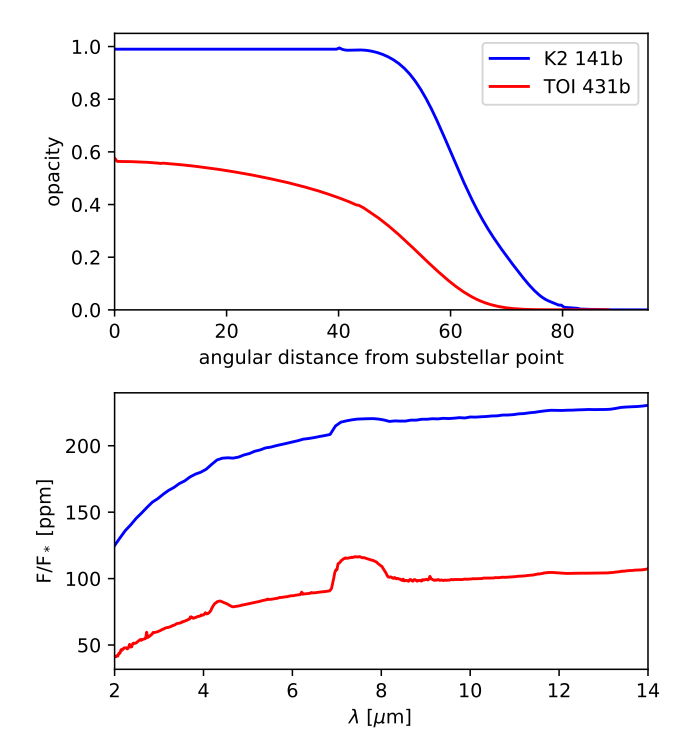


FIG. 4.— Total opacity (top) and synthetic eclipse spectra of K2-141b and TOI-431b (bottom). Total opacity is calculated as the fraction of stellar absorption and total bolometric flux. Because most of K2-141b's opacity is roughly unity, the atmosphere radiates like a perfect blackbody resulting in severely muted spectral features. TOI-431b, on the other hand, has significantly lower opacity for its entire atmosphere making atmospheric signals more distinguishable in its eclipse spectrum.

Given the spatial distribution of surface and atmospheric temperatures, we construct a global map of outgoing top-of-atmosphere emission to create a synthetic eclipse emission spectrum. This process is also identical to Nguyen et al. (2024) which itself is based on Cowan & Agol (2008). The eclipse spectra are shown in Fig. 4.

For K2-141b, as seen in Fig. 4, the opacity is near unity until an angular distance of 40°. In this region, the atmosphere and surface have the same temperature and so result in a blackbody spectrum devoid of emission or absorption features. Because distinguishable atmospheric emission comes from only about half of the dayside hemisphere, K2-141b's eclipse spectrum shows very muted atmospheric spectral features.

For TOI-431b, the opacity never exceeds 0.6 so atmospheric temperature and surface temperature differ significantly with the atmosphere being much hotter than the surface. Unlike K2-141b, the entirety of TOI-431b's dayside hemisphere produces an emission feature so its eclipse spectrum shows much more pronounced atmospheric spectral features.

4. IMPLICATIONS

4.1. Dynamics

To gauge the radiative impact of atmospheric composition and abundances, we plot the opacity contributions of each gas species in Fig. 5. Sodium is the most volatile gas species studied and its strong spectral features in the visible contribute to significant atmospheric heating since most of the starlight is visible light. Potassium also

has strong spectral features in the visible but is not as abundant as Na. Therefore, the contribution to opacity by K follows the same trend as Na but is generally 30% lower.

An unexpected major contributor to opacity is MgO. It has relatively weak spectral features but the features are broad, encompassing much of the visible and IR. For TOI-431b, MgO abundances are not high enough for lines to be saturated. Conversely, K2-141b has enough atmospheric MgO to saturate IR and visible lines, which makes the atmosphere completely opaque at all wavelengths. Because other gases have relatively narrow spectral peaks, MgO dominates atmospheric opacity in high-temperature lava planets.

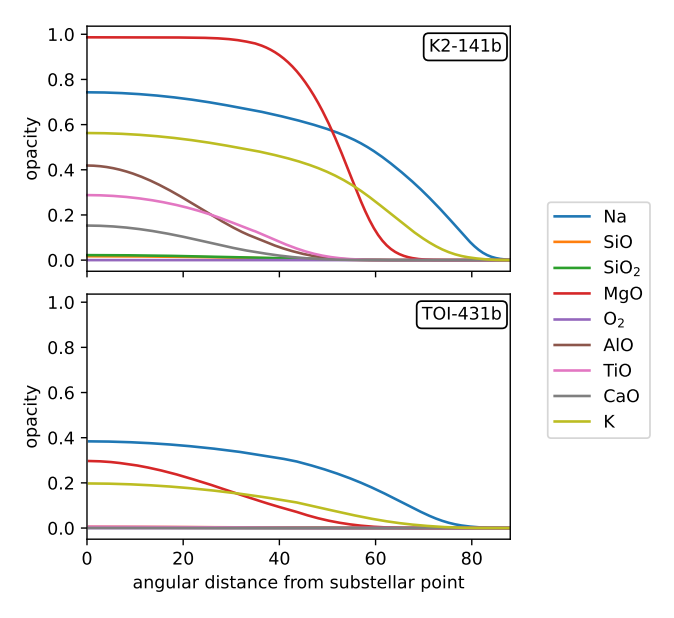


Fig. 5.— Opacity contribution of individual gas species on K2-141b (top) and TOI-431b (bottom). For thin atmospheres like TOI-431b with substellar surface pressures of $\sim 10^3$ Pa, Na and K are the main contributor of stellar flux absorption. Given a thick enough atmosphere like K2-141b's, there is enough MgO ($\sim 10^2$ Pa) to absorb all incoming stellar radiation.

For hot planets with substellar temperatures around 3000 K such as K2-141b, their atmospheres are virtually opaque. Dynamically, this results in a vertically isothermal atmosphere around the substellar region which transitions to a temperature inversion towards the terminator. For cooler planets with surface substellar temperatures around 2500 K like TOI-431b, the atmosphere should have an inversion everywhere on the planet, consistent with Zilinskas et al. (2022).

Nguyen et al. (2022) showed that when the atmosphere has relatively inefficient IR cooling, temperatures must rise to emit more shortwave radiation and maintain radiative balance. Because the optical depth of rock vapour is strongest in the visible, optically thin atmospheres become hotter than the surface thus producing a significant temperature inversion. This suggests that convection is severely inhibited for cool lava planets implying that these atmospheres stratify easily and cloud formation is suppressed. In contrast, optically thick atmospheres from hotter lava planets are isothermal and thus more convectively stable, leading to more opportunities

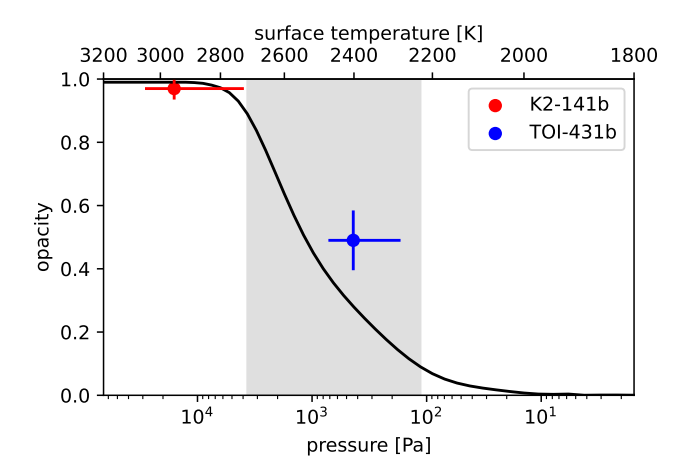


FIG. 6.— Opacity as a function of surface temperature and pressure determined via the stellar spectrum of K2-141. The grey area highlights where opacity is between 0.1 and 0.9. The red and blue lines show the opacity and pressure range for the substellar region ($\theta < 50^{\circ}$) of K2-141b and TOI-431b. For opacity greater than 0.9, the atmosphere absorbs and reradiates nearly all fluxes which makes the atmosphere isothermal and inhibits atmospheric detection. For opacity lower than 0.1, the atmosphere is nearly transparent at all wavelengths, which also inhibits spectral features. Therefore, planets with surface temperatures in the grey area (2300 - 2700 K) are optimal for atmospheric detection and characterization.

for heterogeneous cloud nucleation.

4.2. Observability

The conditions around the substellar region that dictate atmospheric dynamics and the opacity in this region is the most important factor for atmospheric detection. An optically thin atmosphere will allow all light to pass through it unimpeded so thermal emission will come from the surface, which should behave like a perfect blackbody given the low albedo of magma (Essack et al. 2020). Conversely, atmospheric opacity near unity will also yield blackbody-like emission. Therefore, the atmospheric characterization window lies at opacities of 0.1-0.9 corresponding to surface temperatures between 2300-2700 K as seen in Fig. 6.

Our results highlight a paradox for atmospheric characterization of lava planets: it is harder to detect a thick atmosphere than a thin atmosphere. As seen in the eclipse spectra of Fig. 4, the hotter K2-141b with 10 times the atmospheric mass shows weaker atmospheric signals than the cooler TOI-431b. This has profound implications for observation strategies.

K2-141b is a popular target for observations because of its high signal-to-noise ratio (Dang et al. 2021; Espinoza et al. 2021). It is also very hot which reinforces confidence that there is an appreciable atmosphere present

to study. However, our work shows that target selection should consider the optical thickness of the atmosphere when the goal is to detect the spectral signature of an atmosphere.

5. CONCLUSIONS

We improved upon past work to build SonicVapour, an open-source code that models the chemically-complex steady-state hydrodynamics of lava planet atmospheres. We then simulate the atmospheres of K2-141b and TOI-431b to test the limiting cases of optically thick and thin atmospheres.

Our results showed that for a thin atmosphere ($\sim 10^3$ Pa), Na and K dominate stellar absorption and the atmosphere exhibits emission features. With a thicker atmosphere ($\sim 10^4$ Pa) like K2-141b, the trace gas MgO becomes abundant enough to dominate radiative transfer and the atmosphere becomes opaque at all wavelengths.

For an opaque atmosphere, top-of-atmosphere emission essentially looks like a perfect blackbody which is indistinguishable from the magma. Counter-intuitively, an atmosphere needs to be thin enough to produce a significant atmospheric signal. This result suggests a paradigm shift for lava planet observations which should focus on somewhat cooler planets to characterize their atmospheres.

There are many avenues to further use and expand SonicVapour. Although we used a Bulk Silicate Earth composition, this could be expanded to any magma composition admitted by chemical equilibrium models like LavAtmos. Therefore, one could use interior models from Boukaré et al. (2025) or Nicholls et al. (2024) to determine the changes in atmospheric conditions as the magma ocean cools and differentiates. One could also arbitrarily remove volatiles like Na from the atmosphere to mimic cold-trapping (Nguyen et al. 2020) or hydrodynamical escape (Ito & Ikoma 2021). One could also implement Coriolis forces given the results of Lai et al. (2024) to better spatially resolve the atmosphere. These improvements would improve the fidelity of our simulations of lava planet atmospheres.

ACKNOWLEDGMENTS

This research was partially funded by the Canadian Space Agency's James Webb Space Telescope observer's program and the Heising-Simons Foundation. N.B.C. acknowledges support from an NSERC Discovery Grant, a Tier 2 Canada Research Chair, and an Arthur B. McDonald Fellowship. The authors also thank the Trottier Space Institute and l'Institut de recherche sur les exoplanètes for their financial support and dynamic intellectual environment.

REFERENCES

Boukaré, C.-É., Badro, J., & Samuel, H. 2025, Nature, 1 Castan, T., & Menou, K. 2011, The Astrophysical Journal Letters, 743, L36

Chandrasekhar, S. 1947, Bulletin of the American Mathematical Society, 53, 641

—. 1960, Radiative transfer (Courier Corporation)

Chao, K.-H., deGraffenried, R., Lach, M., et al. 2021, Geochemistry, 81, 125735

Cowan, N. B., & Agol, E. 2008, The Astrophysical Journal, 678, L129 Dang, L., Cowan, N. B., Hammond, M., et al. 2021, JWST Proposal. Cycle 1, 2347

Espinoza, N., Bello-Arufe, A., Buchhave, L. A., et al. 2021, JWST Proposal. Cycle 1, 2159

Essack, Z., Seager, S., & Pajusalu, M. 2020, The Astrophysical Journal, 898, 160

France, K., Loyd, R. P., Youngblood, A., et al. 2016, The Astrophysical Journal, 820, 89

Holland, H. D., & Turekian, K. K. 2003, Treatise on geochemistry: 8. Biogeochemistry

- Ingersoll, A. P., Summers, M. E., & Schlipf, S. G. 1985, Icarus, $64,\,375$
- Ito, Y., & Ikoma, M. 2021, Monthly Notices of the Royal Astronomical Society, 502, 750
- Kite, E. S., Fegley Jr, B., Schaefer, L., & Gaidos, E. 2016, The Astrophysical Journal, 828, 80
- Lai, Y., Kang, W., & Yang, J. 2024, The Planetary Science Journal, 5, 205
- Lopez, E. D., Fortney, J. J., & Miller, N. 2012, The Astrophysical Journal, 761, 59
- Malavolta, L., Mayo, A. W., Louden, T., et al. 2018, The Astronomical Journal, 155, 107
- Mollière, P., Wardenier, J., Van Boekel, R., et al. 2019, Astronomy & Astrophysics, 627, A67
- Monaghan, C., Roy, P.-A., Benneke, B., et al. 2025, The Astronomical Journal, 169, 239
- Nguyen, T. G., Cowan, N. B., Banerjee, A., & Moores, J. E. 2020, Monthly Notices of the Royal Astronomical Society, 499, 4605
- Nguyen, T. G., Cowan, N. B., & Dang, L. 2024, The Astronomical Journal, 168, 287
- Nguyen, T. G., Cowan, N. B., Pierrehumbert, R. T., Lupu, R. E., & Moores, J. E. 2022, Monthly Notices of the Royal Astronomical Society, 513, 6125

This paper was built using the Open Journal of Astrophysics IATEX template. The OJA is a journal which

- Nicholls, H., Lichtenberg, T., Bower, D. J., & Pierrehumbert, R. 2024, Journal of Geophysical Research: Planets, 129, e2024JE008576
- Osborn, A., Armstrong, D. J., Cale, B., et al. 2021, Monthly Notices of the Royal Astronomical Society, 507, 2782
- Patel, J. A., Brandeker, A., Kitzmann, D., et al. 2024, Astronomy & Astrophysics, 690, A159
- Schaefer, L., & Fegley, B. 2009, The Astrophysical Journal, 703, L113
- Tennyson, J., & Yurchenko, S. N. 2012, Monthly Notices of the Royal Astronomical Society, 425, 21
- Van Buchem, C. P., Miguel, Y., Zilinskas, M., & van Westrenen, W. 2023, LavAtmos: An open-source chemical equilibrium vaporization code for lava worlds, Wiley Online Library
- Wordsworth, R. 2015, The Astrophysical Journal, 806, 180 Zieba, S., Zilinskas, M., Kreidberg, L., et al. 2022, Astronomy & Astrophysics, 664, A79
- Zilinskas, M., Van Buchem, C., Miguel, Y., et al. 2022, Astronomy & Astrophysics, 661, A126

provides fast and easy peer review for new papers in the astro-ph section of the arXiv, making the reviewing process simpler for authors and referees alike. Learn more at http://astro.theoj.org.